Bioactive Materials 13 (2022) 9–22

Contents lists available at ScienceDirect

Bioactive Materials

journal homepage: www.keaipublishing.com/en/journals/bioactive-materials

Bisphosphonate-based hydrogel mediates biomimetic negative feedback regulation of osteoclastic activity to promote bone regeneration

Zhuo Li [a,1], Haixing Wang [b,1], Kunyu Zhang [c,e,g,h,1], Boguang Yang [a], Xian Xie [a], Zhengmeng Yang [b], Lingchi Kong [d], Peng Shi [e,g], Yuan Zhang [e,g], Yi-Ping Ho [a], Zhi-Yong Zhang [f,**], Gang Li [b,***], Liming Bian [e,g,h,*]

[a] Department of Biomedical Engineering, The Chinese University of Hong Kong, Sha Tin, New Territories, 999077, Hong Kong, China
[b] Department of Orthopaedic and Traumatology, The Chinese University of Hong Kong, Sha Tin, New Territories, 999077, Hong Kong, China
[c] Department of Materials Science and Engineering, Johns Hopkins University, Baltimore, MD, 21218, USA
[d] Department of Orthopaedic Surgery, Affiliated Sixth People's Hospital, Shanghai Jiao Tong University, Shanghai, 200233, China
[e] School of Biomedical Sciences and Engineering, South China University of Technology, Guangzhou, 510006, China
[f] Translational Research Centre of Regenerative Medicine and 3D Printing of Guangzhou Medical University, Guangdong Province Engineering Research Center for Biomedical Engineering, State Key Laboratory of Respiratory Disease, The Third Affiliated Hospital of Guangzhou Medical University, Guangzhou City, Guangdong Province, 510150, China
[g] National Engineering Research Center for Tissue Restoration and Reconstruction, South China University of Technology, Guangzhou, 510006, China
[h] Key Laboratory of Biomedical Materials and Engineering of the Ministry of Education, South China University of Technology, Guangzhou, 510006, China

ARTICLE INFO

Keywords:
Bisphosphonate
Hydrogel
Tissue engineering
Bone regeneration

ABSTRACT

The intricate dynamic feedback mechanisms involved in bone homeostasis provide valuable inspiration for the design of smart biomaterial scaffolds to enhance in situ bone regeneration. In this work, we assembled a biomimetic hyaluronic acid nanocomposite hydrogel (HA-BP hydrogel) by coordination bonds with bisphosphonates (BPs), which are antiosteoclastic drugs. The HA-BP hydrogel exhibited expedited release of the loaded BP in response to an acidic environment. Our *in vitro* studies showed that the HA-BP hydrogel inhibits mature osteoclastic differentiation of macrophage-like RAW264.7 cells via the released BP. Furthermore, the HA-BP hydrogel can support the initial differentiation of primary macrophages to preosteoclasts, which are considered essential during bone regeneration, whereas further differentiation to mature osteoclasts is effectively inhibited by the HA-BP hydrogel via the released BP. The *in vivo* evaluation showed that the HA-BP hydrogel can enhance the in situ regeneration of bone. Our work demonstrates a promising strategy to design biomimetic biomaterial scaffolds capable of regulating bone homeostasis to promote bone regeneration.

1. Introduction

Bone homeostasis is regulated by coupling bone resorption with bone formation, which is of great significance for the renewal of bone components, the repair of injury, and the maintenance of bone structure and mechanical properties [1–4]. In this balanced process, osteoblasts synthesize nonmineralized bone matrix [5–9]. Moreover, preosteoclasts secrete anabolic factors, including PDGF-BB, TGF-β, and IGF-1, to promote bone formation [10–14], whereas mature osteoclasts produce catabolic factors, including cathepsin K and tartrate resistant acid phosphatase (TRAP), and create acidic subosteoclastic compartments to mediate bone resorption [15–20]. During homeostasis, bone resorption due to increased activity of mature osteoclasts under increased RANKL exposure leads to the release of matrix-bound factors, including IGF-1 and TGF-β, triggering the recruitment of osteoblasts and their production of OPG, which can inhibit RANKL and the associated activity of mature osteoclasts (Scheme. 1A) [21–26]. This negative feedback mechanism is the key to maintain bone homeostasis.

Peer review under responsibility of KeAi Communications Co., Ltd.
* Corresponding author. School of Biomedical Sciences and Engineering, South China University of Technology, Guangzhou, 510006, China.
** Corresponding author.
*** Corresponding author.
E-mail addresses: drzhiyong@126.com (Z.-Y. Zhang), gangli@cuhk.edu.hk (G. Li), bianlm@scut.edu.cn (L. Bian).
[1] These authors contributed equally to this work.

https://doi.org/10.1016/j.bioactmat.2021.11.004
Received 25 August 2021; Received in revised form 4 November 2021; Accepted 4 November 2021
Available online 12 November 2021

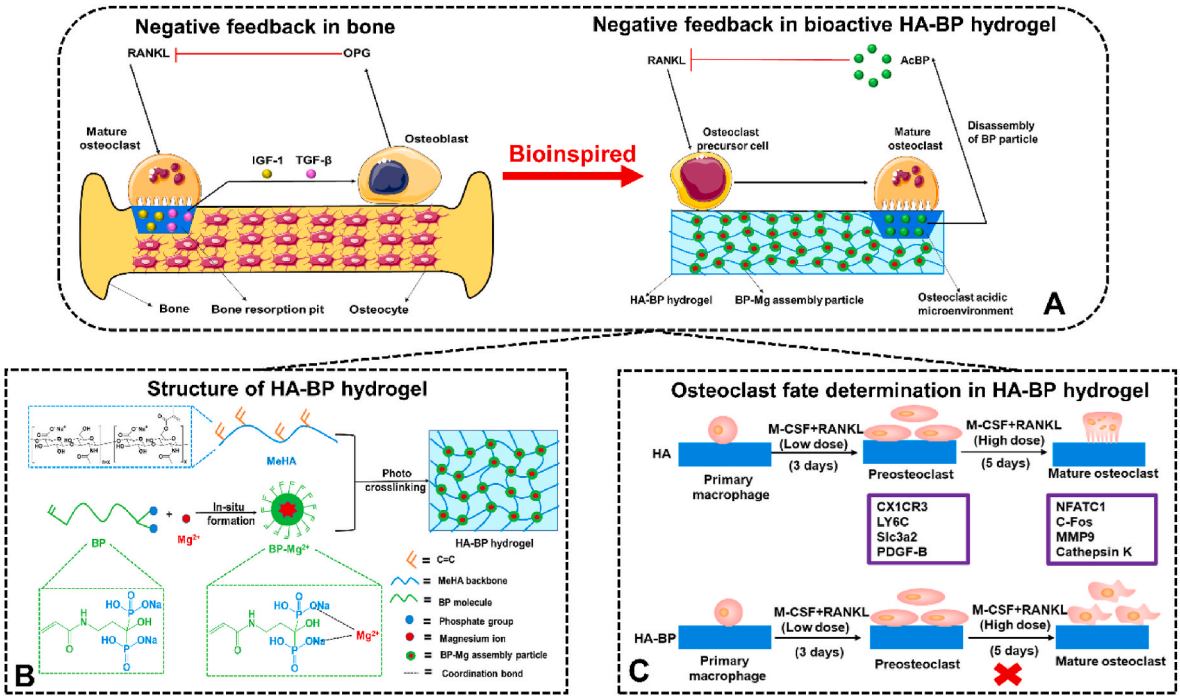

Scheme 1. HA-BP hydrogel mediates negative feedback regulation of osteoclastic activity for enhanced bone regeneration. (A) Native negative feedback regulation of osteoclasts in bone. Under homeostatic conditions, bone resorption due to the elevated activity of mature osteoclasts under increased RANKL exposure leads to the release of matrix-bound factors, including IGF-1 and TGF-β, triggering the recruitment of osteoblasts and their production of OPG, which could inhibit RANKL-induced osteoclast maturation [47,48]. Biomimetic emulation of the negative feedback regulation of osteoclasts by HA-BP hydrogel. Osteoclastic activities degrade the HA-BP hydrogel, thereby triggering the release of BP, which in turn inhibits RANKL-induced osteoclastic maturation. (B) The structure of the HA-BP hydrogel. The coordination bond between magnesium ions and acryloyl bisphosphonate leads to nanoparticle self-assembly followed by further photo-crosslinking with MeHA. (C) The different cell fates of the control BP-free HA and HA-BP hydrogels. In the HA hydrogel without BP, primary macrophages can differentiate into preosteoclasts and further develop into mature osteoclasts. However, in the HA-BP hydrogel group, primary macrophages can differentiate into preosteoclasts, which contribute to bone formation, but cannot form bone-absorbing mature osteoclasts.

The remarkable dynamic regulation of bone homeostasis can provide valuable inspiration for the design of biomaterial scaffolds, which have demonstrated valuable functions in addressing various bone injuries and diseases. Bisphosphonates have emerged as a promising building block for fabricating bioactive biomaterial scaffolds for bone regeneration [27–32]. BPs are a class of drugs with inhibitory effects on osteoclastic activity and bone resorption [33–39]. BPs not only promote apoptosis and inhibit the activity of osteoclasts but also interfere with the reception of bone resorption signals from the bone matrix by osteoclasts [40–42]. However, few prior studies have examined the potential of BP-based biomaterials to emulate the negative feedback properties of the native bone matrix to regulate bone homeostasis and promote bone regeneration. In this study, we developed a bisphosphonate-based nanocomposite hyaluronic acid hydrogel (HA-BP) containing self-assembled nanostructures based on BP–magnesium coordination (Scheme. 1B). The HA-BP hydrogel can mediate the expedited release of BP in response to an acidic environment, which can be generated by mature osteoclastic activity. We demonstrated that the HA-BP hydrogel supports preosteoclastic differentiation, which is important for bone regeneration, but inhibits the further osteoclastic maturation of primary macrophages via the triggered release of BP (Scheme. 1C). Prior studies have reported that direct supplementation of BP inhibited both pre-osteoclast and mature osteoclast without selectivity [43–46]. However, our hydrogel only releases basal level of BP in the presence of pre-osteoclasts but releases substantial amount of BP in the presence of mature osteoclasts which are known to form the acidic subosteoclastic compartment. This acidity-dependent BP release kinetics from our hydrogel may contribute to the selective inhibition of mature osteoclasts. We further showed that the implantation of HA-BP hydrogel in animal bone defects promoted the in situ regeneration of bone. We believe that this study provides a promising design strategy for smart biomaterials to selectively suppress mature osteoclastic activity for enhanced bone regeneration.

2. Materials and methods

2.1. Materials

Sodium hyaluronate was purchased from Bloomage BioTechnology Corporation Limited (JiNan, China). Methacrylic anhydride was obtained from J&K Chemicals (Beijing, China). Sodium hydroxide, absolute ethanol, hydrochloric acid, formaldehyde, chloroform, isopropanol, polyformaldehyde, and Tween 20 were purchased from Sigma-Aldrich (USA). Sodium chloride was purchased from Aladdin (Shanghai, China). Pamidronate disodium was purchased from Meilun Biotechnology Corporation Limited (Dalian, China). *N*-Acryloxysuccinimide was obtained from J&K Chemicals (Beijing, China). Magnesium chloride was purchased from Macklin (Shanghai, China). 2-Hydroxy-4'-(2-hydroxyethoxy)-2-methylpropiophenone (I2959) was purchased from J&K Chemicals (Beijing, China). Twenty-four-well cell culture plates and cell scrapers were obtained from SPL Life Science Corporation Limited (Korea). PBS, DMEM, FBS, penicillin-streptomycin, 4′,6-diamidino-2-phenylindole (DAPI), Alamar blue, and TRIzol reagent were purchased from Thermo Fisher (USA). Rhodamine phalloidin was purchased from Cytoskeleton (USA). M-CSF and Annexin V-FITC/7-AAD cell apoptosis kits were purchased from Sinobiological (Beijing, China). Recombinant mouse TRANCE/RANK L/TNFSF11 (*E. coli*-expressed) was purchased from R&D (USA). The Acid Phosphatase, Leukocyte (TRAP) Kit was purchased from Sigma-Aldrich (USA). TB Green Premix Ex Taq (Tli RNase H Plus) and PrimeScript RT Master Mix were purchased from

TaKaRa (JAPAN). The F4/80 (sc-52664), PDGF-BB (sc-365805), ALP (sc- 271431), NFATc1 (sc-7294), cathepsin K (sc-48353), Col I (sc-59772), and OCN (sc-390887) primary antibodies were purchased from Santa Cruz (USA). The TRAP (11594-1-AP) primary antibody was purchased from Proteintech (Wuhan, China). The goat anti-mouse secondary antibody was purchased from Thermo Fisher (USA). All primers were synthesized by Shanghai Generay Biotechnology Corporation Limited (Shanghai, China). A Tartrate Resistant Acid Phosphatase Assay Kit was purchased from Beyotime Biotechnology Corporation Limited (Shanghai, China). Farnesyl diphosphate synthase and geranylgeranyl diphosphate synthase activity kits were purchased from MyBioSource (USA). PDGF-BB activity kit was purchased from Solarbio Science & Technology Co., Ltd (Beijing, China). ALP enzymatic activity kit was purchased from Solarbio Science & Technology Co., Ltd (Beijing, China). An H&E staining kit was purchased from Biosharp (Hefei, China). The DAB Peroxidase (HRP) Substrate kit and Vectastain ABC reagent kit were purchased from Vector Laboratories (USA).

2.2. Synthesis of acrylated bisphosphonate (AcBP)

Pamidronate disodium and *N*-acryloxysuccinimide were dissolved together in deionized water at a final concentration of 5 mM. This reaction solution was adjusted to pH 8.0 with sodium hydroxide and stirred for 24 h at room temperature. After the reaction, the final product solution was added dropwise to absolute ethanol. The final product was precipitated and washed with ethanol three times. Finally, the precipitate was dried in a vacuum drying oven for 2 days. The final product was characterized by NMR.

2.3. Synthesis of methacrylated sodium hyaluronate (MeHA)

Sodium hyaluronate (HA) was dissolved in deionized water at a mass fraction of 1% and stirred for 3 h. Methacrylic anhydride was added dropwise to the HA solution with a volume fraction of 1.2%. The reaction solution was continually adjusted to pH 8.0–8.5 with sodium hydroxide for 8 h. Then, the reaction solution was dialyzed with sodium chloride for 3 days and deionized water for another 3 days. Finally, the reaction solution was lyophilized and characterized by NMR.

2.4. Fabrication and rheological characterization of the HA-BP hydrogel

MeHA was dissolved in PBS (pH 7.4) at a mass fraction of 2%. BP was dissolved in PBS (pH 7.4) at a final concentration of 100 mM. Next, magnesium chloride was added to the mixture at a final concentration of 100 mM. Then, the photoinitiator I2959 was added to the mixture with a mass fraction of 0.05%. This gel precursor solution was added to the glass plate of the rheometer. Under UV light stimulation for 10 min, the HA-BP hydrogel formed in situ on the glass plate. The grafting rate of BP is estimated to be around 97%. The Young's modulus of HA-BP hydrogels was characterized by vertical compression. Then, MeHA was dissolved in PBS (pH 7.4) at a mass fraction of 2%. The photoinitiator I2959 was added to the solution with a mass fraction of 0.05%. This gel precursor solution was stimulated under UV light for 30 min to form the HA hydrogel. The Young's modulus characterization was also performed on the HA hydrogel.

2.5. Biocompatibility of the HA-BP hydrogel

Fourth generation RAW264.7 macrophages were cultured in DMEM with 10% FBS and 1% penicillin-streptomycin for 3 days to become the fifth generation of cells. HA and HA-BP 2D hydrogels were fabricated according to section 2.4. The fifth generation of cells was seeded on hydrogels at a density of 20000/well. Cells were cultured in DMEM with 10% FBS and 1% penicillin-streptomycin. Microscopic images were acquired every day. On days 1, 3, and 5, Alamar blue activity was detected according to the manufacturer's protocol. After 6 days, the cells were fixed with 4% (w/v) polyformaldehyde (PFA) for 1 h. Then, the cells were treated with 0.25% (v/v) Triton X-100 for 30 min. Next, the cells were washed with PBS (pH 7.4) 3 times. Finally, the cells were treated with phalloidin (1:400, Thermo Fisher) for 1 h and DAPI (1:1000, Thermo Fisher) for 20 min. Immunofluorescence images were obtained by confocal microscopy (Nikon).

2.6. Controlled release of AcBP from the HA-BP hydrogel

A stock BP standard solution (1 mM) was prepared in PBS (pH 7.4). Through dilution with PBS (pH 7.4), a series of BP solutions with different concentrations (0.001, 0.005, 0.01, 0.02, 0.05, 0.1, 0.2 mM) were obtained. The detection wavelength is 207 nm. The standard curve of BP was constructed. The HA-BP 2D hydrogels were fabricated on cover slips, which were placed into a 24-well plate. Then, 500 μL of PBS (pH 7.4) was added into wells. The PBS solution (pH 7.4) was changed every day. After 7 days, all samples were collected and measured by UV–Vis spectroscopy. Additionally, the HA-BP 2D hydrogels were soaked in PBS at different pH values. The following equation indicated the release amount per day. The data was presented by cumulative amount.

$$\mathrm{Re}lease\ amount\frac{Y-0.0321}{6.2186}*0.0005(mmol)$$

Y—Absorbance of sample

2.7. RAW264.7 macrophages osteoclastogenesis

Fourth-generation RAW264.7 macrophages were cultured in DMEM with 10% FBS and 1% penicillin-streptomycin for 3 days to become fifth-generation cells. The cells were seeded on HA and HA-BP hydrogels at a density of 20000 cells/well and adhered to the hydrogels for 24 h. Then, the medium was changed every day to medium with RANKL at a final concentration of 30 ng/mL. After 5 days, the hydrogels were collected for further experiments.

2.8. pH variations in the HA and HA-BP medium seeded with RAW264.7 macrophages

RAW264.7 macrophage osteoclastogenesis was performed according to section 2.7. On day 0, day 3, and day 5, medium color variation images were obtained. Additionally, the pH values of the medium were measured with pH meters.

2.9. Primary macrophages osteoclastogenesis

C57BL/c male mice (6–8 weeks) were euthanized by cervical dislocation. The femurs and tibias were separated under sterile conditions and washed in α-MEM with 10% FBS and 1% penicillin-streptomycin for two times. Then, the two ends of femurs and tibias were cut, and the bone marrow was extracted. The obtained bone marrow flowed through a cell strainer to remove some small mouse tissues. Cells were cultured in α-MEM with 10% FBS and 1% penicillin-streptomycin for 12 h. Next, floating cells were collected and further induced by M-CSF at a final concentration of 30 ng/mL to obtain primary macrophages. Primary macrophages were induced to differentiate into preosteoclasts under stimulation with 30 ng/mL M-CSF and 60 ng/mL RANKL for 3 days. The preosteoclasts were further induced to mature osteoclasts by 30 ng/mL M-CSF and 200 ng/mL RANKL for another 5 days.

2.10. TRAP staining and activity

For the TRAP staining experiment, the 2D hydrogel samples were fixed with fixative solution (25% citrate solution, 65% acetone, 10%

formaldehyde) for 1 min and rinsed with PBS (pH 7.4) 3 times. Then, the samples were immersed in staining solution (as prepared according to the manufacturer's protocol) for 1 h at 37 °C. Next, the samples were washed with PBS (pH 7.4) 3 times. Microscopic images were taken of each sample.

For TRAP activity, *para*-nitrophenyl phosphate (pNPP), a common substrate of phosphatase, was used. para-Nitrophenol (*p*-nitrophenol) is produced by the action of acid phosphatase under acidic conditions. para-Nitrophenol (*p*-nitrophenol) is a yellow product under alkaline conditions, and its absorbance can be measured at 400–415 nm. The deeper the yellow color of the product, the higher the acid phosphatase activity. TRAP activity was detected according to the manufacturer's protocol.

2.11. Real-time quantitative PCR

Total RNA was extracted by TRIzol reagent. The concentrations of RNA were detected with a Nanodrop instrument (Thermo Fisher). Five hundred nanograms of mRNA was reverse transcribed to cDNA using PrimeScript RT Master Mix. The primers sequences are shown in Table S1. RT-qPCR was performed by using TB Green Premix Ex Taq (Tli RNase H Plus) on the Applied Biosystem. The running procedures were set according to the manufacturer's protocol. GAPDH was the housekeeping gene. The relative marker gene expression was calculated using the $2^{-\Delta\Delta CT}$ method.

2.12. Immunofluorescent staining

After osteoclastogenesis, the cells were fixed with 4% (w/v) polyformaldehyde (PFA) for 1 h and treated with 0.25% (v/v) Triton X-100 for 30 min. Next, the cells were blocked with 1% FBS for 2 h. Primary antibodies against NFATC1, cathepsin K, PDGF-B and ALP (1:200) were incubated with cells at 4 °C for 16 h. Then, the cells were treated with goat anti-mouse secondary antibody (1:400) at room temperature for 2 h. Finally, the cells were incubated with phalloidin (1:400) for 1 h and DAPI (1:1000) for 30 min. Immunofluorescence images were obtained by confocal microscopy (Nikon). The fluorescence intensity was analyzed by using Image J software.

2.13. Annexin V-FITC/7-AAD staining of osteoclasts apoptosis

Annexin V-FITC and 7-AAD are fluorescent dyes for effective cell apoptosis observation. After macrophage adhesion ($RANKL^-$), the cells were stained with double-fluorescence staining according to the manufacturer's protocol. Immunofluorescence images were obtained by confocal microscopy (Nikon). Additionally, the cells treated with 30 ng/mL RANKL for 3 days were also stained ($RANKL^+$). The percentages of Annexin V and 7-AAD positive cells were estimated by using Image J software.

2.14. Farnesyl diphosphate synthase (FPPS) and geranylgeranyl diphosphate synthase (GGPPS) activity

Fourth-generation RAW264.7 macrophages were cultured in DMEM with 10% FBS and 1% penicillin-streptomycin for 3 days to become fifth-generation cells. The cells were seeded on HA and HA-BP hydrogels at a density of 20000 cells/well and adhered to the hydrogels for 24 h. Then, the medium was changed every day to medium with RANKL at a final concentration of 30 ng/mL. After 5 days, the culture media ($n = 5$ for each group) were collected. FPPS and GGPPS activity were detected by ELISA. ELISA was performed according to the manufacturer's protocol.

2.15. Preosteoclast condition medium analysis

Primary macrophages were induced to differentiate into preosteoclasts under stimulation with 30 ng/mL M-CSF and 60 ng/mL RANKL for 3 days. After 3 days, medium was collected. PDGF-BB activity was detected by ELISA. ELISA was performed according to the manufacturer's protocol.

2.16. ALP activity

Third-generation rat mesenchymal stem cells (rMSCs) were seeded on 12-well plate at a density of 200000 cells/well in α-MEM with 20% FBS, 1% glutamine, and 1% penicillin-streptomycin for 2 days. 1 mL preosteoclast condition medium was added in the 12-well plate to induce osteogenesis of rMSCs for another 3 days. The ALP activity was performed according to the manufacturer's protocol.

2.17. Fabrication of the 3D HA and HA-BP porous hydrogels

Polymethyl methacrylate (PMMA) microspheres were added to a chamber of 1 mL syringe at a volume of 40 μL. HA and HA-BP porous hydrogels were fabricated by dithiothreitol (DTT) crosslinking. For the 3D HA porous hydrogel, MeHA was dissolved in PBS (pH 7.4) at a mass fraction of 2.5%. DTT was dissolved in the MeHA solution at a final concentration of 32 mM to form the gel precursor solution. This precursor solution was infiltrated through the PMMA microspheres to form HA scaffolds. For the 3D HA-BP porous hydrogel, MeHA was dissolved in PBS (pH 7.4) at a mass fraction of 2.5%. BP was dissolved in PBS (pH 7.4) at a final concentration of 100 mM. Next, magnesium chloride was added to the mixture at a final concentration of 100 mM. DTT was dissolved in the mixture at a final concentration of 32 mM to form the gel precursor solution. This precursor solution was infiltrated through the PMMA microspheres to form HA-BP scaffolds. These scaffolds were soaked in acetone overnight to remove the PMMA microspheres. The collected scaffolds were sterilized with 75% ethanol and rinsed with PBS (pH 7.4). The Young's modulus of HA and HA-BP hydrogels was characterized by vertical compression. The 3D HA and HA-BP porous hydrogels were implanted into the subsequent bone defect repair model.

2.18. Rat bone defect repair model

Ethics approval was obtained from the Animal Experimentation Ethics Committee of Chinese University of Hong Kong (AEEC No. 21/026/MIS-5-C). Nine male Sprague-Dawley rats (6–8 weeks) were divided into three groups and raised in an animal house for one week before the operation. Each rat was performed anesthesia by xylazine (4 mg/kg) and ketamine (40 mg/kg). Two 5 mm diameter calvarial defects were created in each rat. The HA and HA-BP 3D porous hydrogels were implanted into the defect sites ($n = 6$ for each group). Defects receiving no hydrogel implantation were used as the blank control group. After 8 weeks, the rats were sacrificed. Cranial bone samples were collected, and microCT analysis was performed. Then, these samples were decalcified in 10% EDTA (pH 7.4) for 1 month, and further immunohistochemical analysis was performed.

2.19. Immunohistochemical staining

The decalcified samples were fixed, dehydrated, made xylene-transparent, wax-dipped and embedded in paraffin. For H&E staining, the histological sections (5 μm) were dewaxed and immersed in hematoxylin staining solution for 3 min and eosin staining solution for 45 s. Finally, the histological sections were mounted in mounting media. For PDGF-B, TRAP, Col I, and OCN immunohistochemical staining, the sections were treated with primary antibodies and peroxidase-conjugated secondary antibodies. The signals were detected with a DAB kit. Immunohistochemical staining was analyzed by using Image J software.

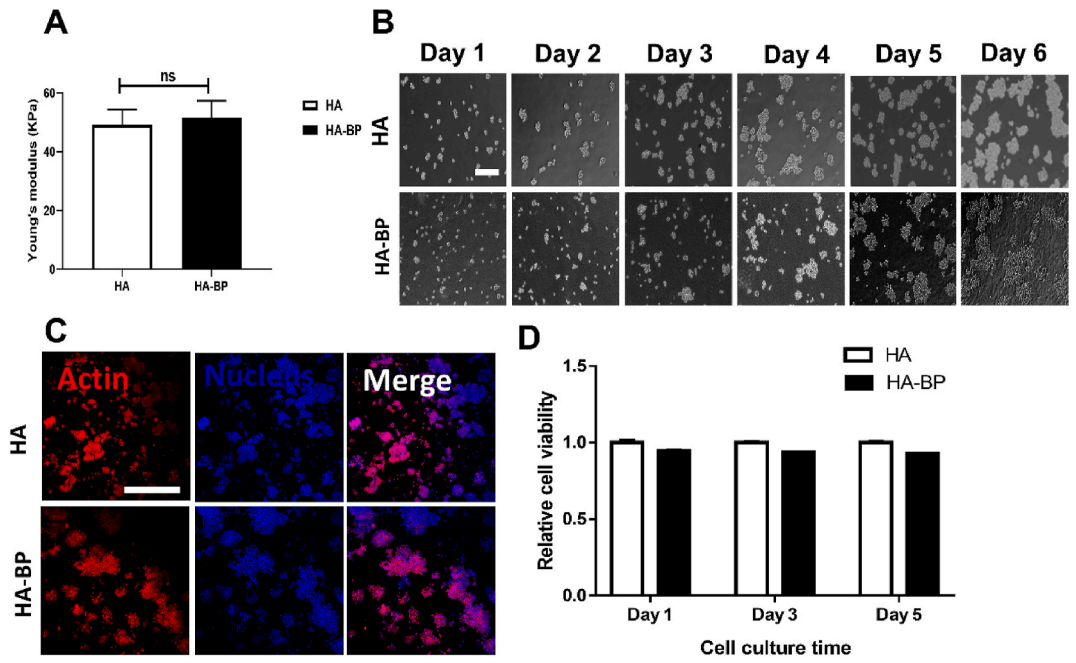

Fig. 1. Cytocompatibility evaluation of the HA-BP hydrogel with macrophages. (A) Young's modulus of HA and HA-BP hydrogels. (B) Microscopic images of RAW264.7 macrophages cultured on HA and HA-BP hydrogel substrates for 6 days. Scale bar = 200 μm. (C) DAPI/actin staining of macrophages cultured on the HA and HA-BP hydrogels after 6 days of culture. Scale bar = 50 μm. (D) Quantitative results of the Alamar Blue assay obtained on days 1, 3, and 5 of culture.

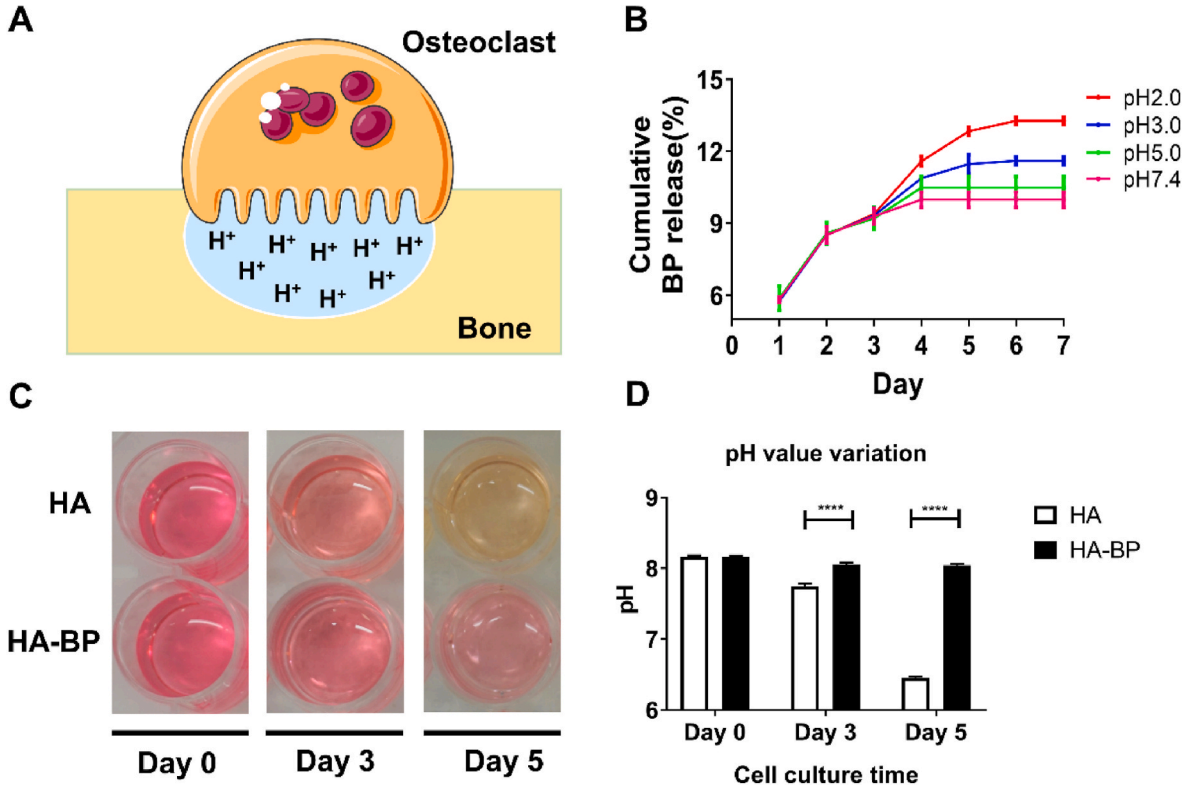

Fig. 2. pH-responsive release of BP from the HA-BP hydrogel. (A) Mature osteoclasts secrete abundant hydrogen ions into the subosteoclastic compartment to lower the local pH and trigger degradation of the bone matrix. (B) Cumulative release of BP from the HA-BP hydrogels incubated in buffer solutions with different pH values (2.0, 3.0, 5.0, 7.4) for 7 days as determined by UV–Vis analysis. All data are presented as the means ± SD (n = 3). (C) The color and (D) pH of the culture medium of RAW264.7 macrophages seeded on HA or HA-BP hydrogels under sustained RANKL stimulation on days 0, 3, and 5. All data are presented as the means ± SD (n = 6).

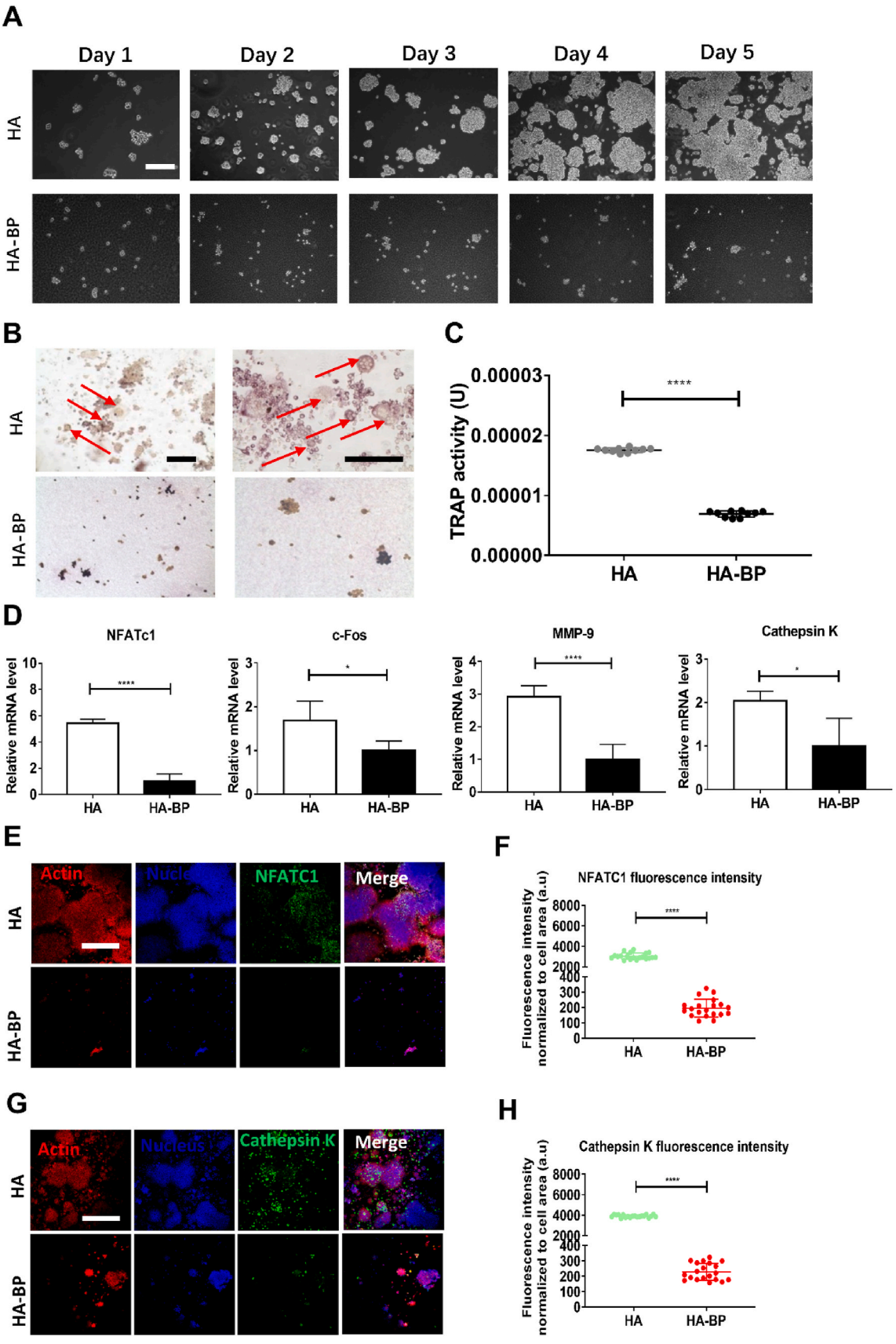

(caption on next page)

Fig. 3. The HA-BP hydrogel inhibits RAW264.7 macrophages osteoclastogenesis. (A) Microscopic images of RAW264.7 macrophages cultured on the HA and HA-BP hydrogels for 5 days of osteoclastic induction with RANKL supplementation. Scale bar = 200 μm. (B) TRAP staining of macrophages cultured on the HA and HA-BP hydrogels on day 5. The red arrows indicate mature multinuclear osteoclasts. Scale bar (left panel and right panel) = 200 μm. (C) Quantification of the TRAP activity of the cells from the HA and HA-BP groups. (D) The expression of osteoclastic marker genes by macrophages cultured on HA and HA-BP hydrogels supplemented with RANKL. qPCR data are presented as the means ± SD (n = 4). *p < 0.05, **p < 0.01, ***p < 0.001. (E) Representative images of NFATC1 (green), actin (red), and nucleus (blue) immunostaining. Scare bar = 50 μm. (F) Fluorescence intensity of NFATC1 of HA and HA-BP hydrogels (n = 20). *p < 0.05, **p < 0.01, ***p < 0.001. (G) Representative images of cathepsin K (green), actin (red), and nucleus (blue) immunostaining. Scare bar = 50 μm. (H) Fluorescence intensity of Cathepsin K of HA and HA-BP hydrogels (n = 20). *p < 0.05, **p < 0.01, ***p < 0.001.

2.20. Statistics

All data are presented as the mean ± standard deviation. Statistical analysis was performed by unpaired Student's t-test with GraphPad Prism 8.0 software. A P value lower than 0.05 was considered significant.

3. Results and discussion

3.1. Fabrication of the HA-BP nanocomposite hydrogel

We first synthesized acryloyl bisphosphonate (Ac-BP) based on pamidronate and *N*-acryloxysuccinimide, as confirmed by the characteristic peak of the carbonyl group of Ac-BP in the ^{1}H NMR spectrum (Fig. S1A). Methacrylated hyaluronic acid (MeHA) was synthesized with a methacrylation degree of 21.5% based on a previously developed protocol (Fig. S1B). HA-BP nanocomposite hydrogels were fabricated by photopolymerizing a mixed precursor solution of Ac-BP, MeHA, and Mg cations (Mg^{2+}). The self-assembly of Ac-BP and Mg^{2+} was driven by the coordination bond between BP and Mg^{2+} and led to the formation of Ac-BP–Mg^{2+} nanostructures bearing acryloyl groups, which function as the crosslinkers of the polymer network in the nanocomposite hydrogel (Scheme. 1B). We hypothesized that the HA-BP hydrogel can emulate the negative feedback mechanism of osteoclastic regulation (Scheme. 1A). Specifically, the reduced local pH due to the activity of mature osteoclasts on the nanocomposite hydrogel can lead to partial degradation of the hydrogel and therefore the expedited release of BP, which in turn inhibits osteoclastic activity. To test this hypothesis, we conducted the following experiments.

3.2. Characterization and biocompatibility of the HA-BP hydrogel

Shi et al. reported that covalent incorporation of bisphosphonates (BPs) into HA hydrogel increased the stiffness of the hydrogel in comparison with the unmodified HA hydrogel of the same cross-linking density. In order to rule out this interfering factor, we kept the Young's modulus of HA and HA-BP hydrogels at the around the same level by adjusting the photocrosslinking time. Rheological analysis showed that there was no significant difference in the Young's modulus between the HA-BP hydrogel and HA hydrogel (Fig. 1A). We next evaluated the cytocompatibility of the HA-BP hydrogels in RAW264.7 macrophages by using the BP-free HA hydrogel as the control. The microscopic images showed that the seeded macrophages proliferated extensively on both the HA and HA-BP hydrogels during 6 days of culture, and there was no significant difference in the cell proliferation rate between the two different hydrogel substrates (Fig. 1B). DAPI/actin staining of the seeded macrophages also showed a similar trend of cell proliferation on both hydrogel substrates (Fig. 1C). The results of the Alamar Blue assay also indicated that there was no significant difference between the metabolic activities of the macrophages cultured on HA and HA-BP hydrogels (Fig. 1D). These results demonstrated that the HA-BP hydrogel had no significant inhibitory effect on the proliferation of macrophages.

3.3. The HA-BP hydrogel mediates the pH-dependent release of BP

In bone, mature osteoclasts secrete protons and catabolic enzymes into the subosteoclastic compartment to lower the local pH and trigger the degradation of bone matrix (Fig. 2A) [49,50]. To evaluate the degradation of the HA-BP hydrogel due to osteoclastic activity, we analyzed the release kinetics of BP from the HA-BP hydrogels based on a standard curve constructed from the UV–Vis data of acryloyl BP (Figs. S2A and B). The HA-BP hydrogels showed an initial release of encapsulated BP (approximately 23.2% of the total encapsulated BP) in PBS (pH 7.4) after 2 days but minimal release afterwards (Fig. S2C). Decreasing the pH of the incubation buffer significantly expedited the release of BP. Specifically, the cumulative release of BP from the HA-BP hydrogel at pH 2 was 32.8% higher than that at pH 7.4 after 7 days (Fig. 2B). This could be attributed to the increased partial disassembly of the coordination-stabilized BP–Mg^{2+} nanostructures in the hydrogels in response to the acidic environment. As reported in our previous publication, the HA-BP hydrogel contained BP–Mg^{2+} nanoparticles assembled by Mg ions and AcBP based on BP–Mg^{2+} coordination [51]. Although some BP on the surface of these nanoparticles can be crosslinked with the hydrogel network during the photopolymerization, there are still non-crosslinked BP in the nanoparticles. Therefore, the low pH can induce partial disassembly the BP–Mg^{2+} nanoparticles to release the non-crosslinked BP. Moreover, we observed different medium color variations from the indicator phenol red in macrophage cultures on hydrogel substrates under sustained RANKL stimulation. In the HA hydrogel group, the medium color changed from red to yellow, and the medium acidity increased with increasing culture time due to RANKL-induced osteoclastic maturation and metabolic activity. In contrast, in the HA-BP hydrogel group, despite the sustained stimulation from RANKL, the lack of media color change indicated the minimal medium acidification, which may be associated with mature osteoclastic activity (Fig. 2C and D).

3.4. The HA-BP hydrogel inhibits osteoclastic differentiation of macrophage-like RAW264.7 cells

Mononuclear RAW264.7 macrophages can differentiate into multinuclear mature osteoclasts under RANKL stimulation, and bisphosphonate is known to inhibit this differentiation [52–55]. We cultured macrophages on the HA and HA-BP hydrogel substrates supplemented with RANKL in the medium (Fig. 3A). After 5 days of culture, TRAP staining showed the appearance of multinuclear cells on the HA hydrogel, while there were no multinuclear cells on the HA-BP hydrogel (Fig. 3B). We quantified the activity of tartrate-resistant acid phosphatase (TRAP), a key marker of osteoclastic activity, based on a standard assay (Fig. S3A). We constructed a standard curve by using *p*-nitrophenol as the substrate (Fig. S3B). The TRAP activity of the cells on the HA-BP hydrogel was significantly lower than that of cells on the HA hydrogel (Fig. 3C).

To further verify the inhibitory effects of the HA-BP hydrogel on osteoclastic differentiation, we evaluated the expression of 10 selected marker genes involved in osteoclastogenesis. The qPCR data showed that the expression of all osteoclastic marker genes was significantly downregulated in cells cultured on the HA-BP hydrogel compared with cells cultured on the HA hydrogel (Fig. 3D and Fig. S4). Furthermore, we performed immunofluorescence staining against two key markers of osteoclastogenesis, NFATC1 and cathepsin K. The fluorescence intensities from NFATC1 and cathepsin K staining in the HA-BP group were significantly lower than those in the HA group (Fig. 3E-H). Taken

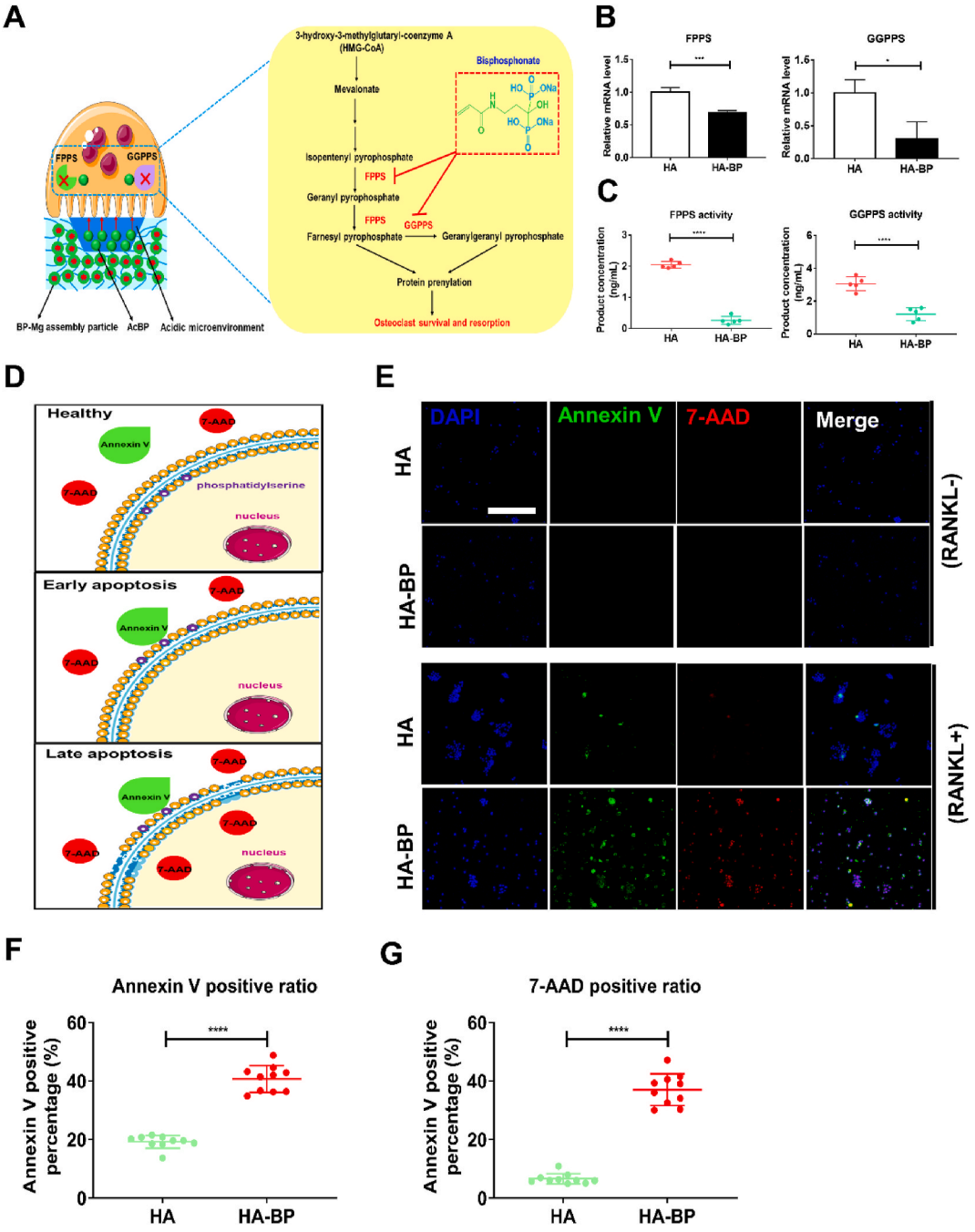

Fig. 4. The HA-BP hydrogel promotes apoptosis of mature osteoclasts. (A) The metabolic pathway of mature osteoclasts. Bisphosphonates inhibits the activities of farnesyl pyrophosphate synthase (FPPS) and geranylgeranyl diphosphate synthase (GGPPS), thereby inhibiting protein prenylation, which is crucial to osteoclast survival and resorption. (B) The expression of FPPS and GGPPS genes in macrophages cultured on the HA and HA-BP hydrogels supplemented with RANKL. qPCR data are presented as the means ± SD (n = 4). *p < 0.05, **p < 0.01, ***p < 0.001. (C) The enzymatic activities of FPPS and GGPPS in macrophages cultured on the HA and HA-BP hydrogels supplemented with RANKL. ELISA data are presented as the means ± SD (n = 5). *p < 0.05, **p < 0.01, ***p < 0.001. (D) A schematic diagram of cell apoptosis. In healthy cells, phosphatidylserine is located in the inner layer of the cell membrane, thereby resulting in no staining by annexin V-FITC or 7-AAD. In early apoptotic cells, phosphatidylserine externalizes from the inner layer to the outer layer of the cell membrane, and cells are stained by annexin V-FITC. Late apoptotic cells are stained by both annexin V-FITC and 7-AAD. (E) Annexin V staining of RAW264.7 macrophages cultured on the HA and HA-BP hydrogels on Day 0 and Day 3. Blue fluorescence indicates cell nuclei, green fluorescence indicates annexin V and red fluorescence indicates 7-AAD. Scare bar = 50 μm. (F) Annexin V positive percentage of HA and HA-BP hydrogels on Day 3 (n = 10). *p < 0.05, **p < 0.01, ***p < 0.001. (G) 7-AAD positive percentage of HA and HA-BP hydrogels on Day 3 (n = 10). *p < 0.05, **p < 0.01, ***p < 0.001.

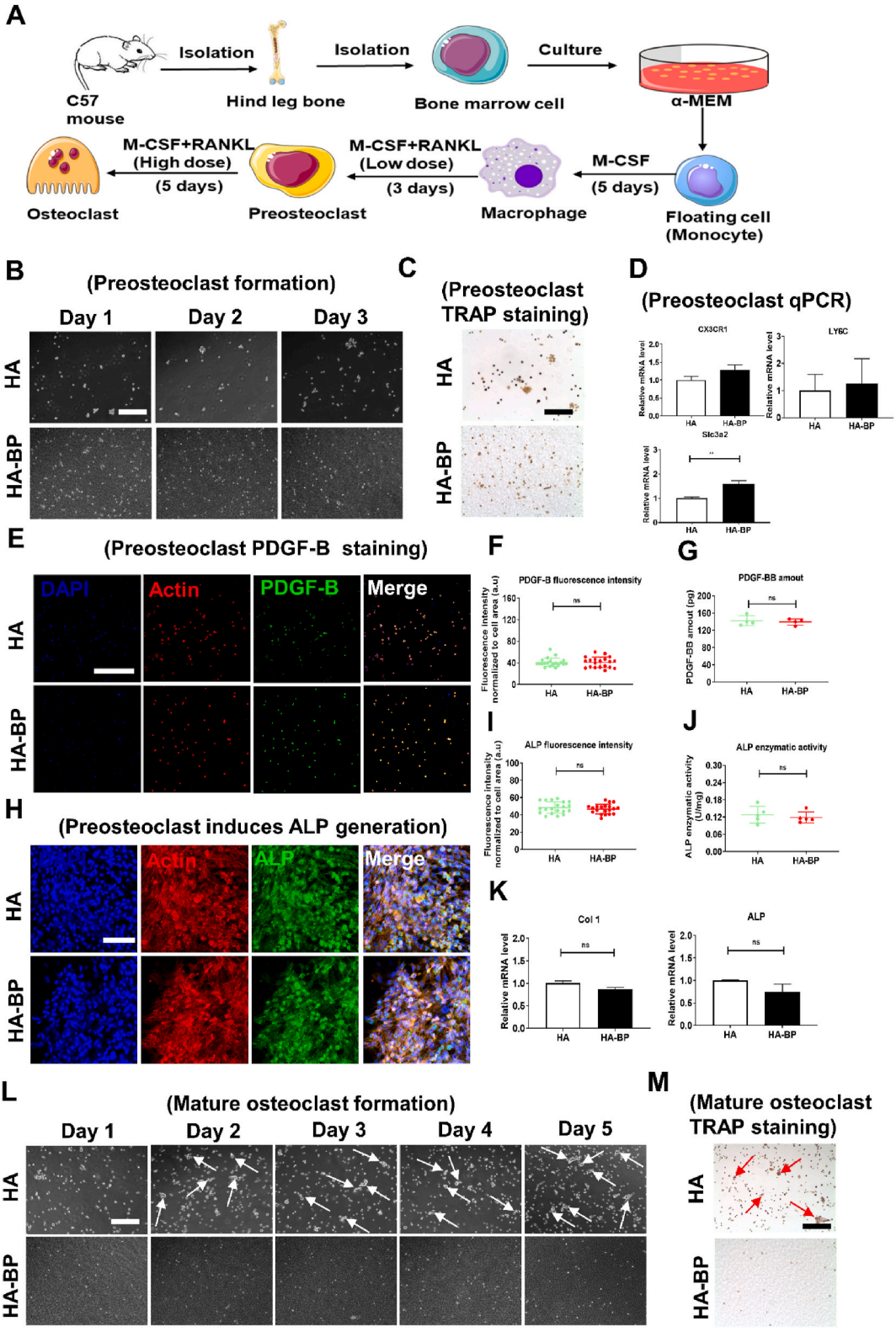

(caption on next page)

Fig. 5. The HA-BP hydrogel supports preosteoclast differentiation but inhibits osteoclast maturation. (A) The process of deriving preosteoclasts and mature osteoclasts from primary macrophages. (B) Microscopic images of cells cultured on the HA and HA-BP hydrogels during 3 days of preosteoclast induction with a low dose of RANKL (30 ng/mL). Scale bar = 200 μm. (C) TRAP staining of preosteoclasts cultured on the HA and HA-BP hydrogels after 3 days of induction with a low dose of RANKL (30 ng/mL). Scale bar = 200 μm. (D) The mRNA levels of preosteoclast marker genes in preosteoclasts after 3 days of culture with a low dose of RANKL (30 ng/mL) on the HA and HA-BP hydrogels. qPCR data are presented as the means ± SD (n = 4). *p < 0.05, **p < 0.01, ***p < 0.001. (E) Representative images of preosteoclast immunostaining against PDGF-B (green), actin (red), and nuclei (blue) after 3 days of induction with a low dose of RANKL. Scale bar = 50 μm. (F) Fluorescence intensity of PDGF-B staining (n=20). * p<0.05, ** p<0.01, *** p<0.001. (G) The PDGF-BB secretion by preosteoclasts developed on the HA and HA-BP hydrogels. ELISA data are presented as the means ± SD (n=5). * p<0.05, ** p<0.01, *** p<0.001. (H) Representative images of ALP staining of rat mesenchymal stem cells (rMSCs) induced by preosteoclast-conditioned medium from HA and HA-BP hydrogel groups. Scale bar = 10 μm. (I) Fluorescence intensity of ALP staining (n=20). * p<0.05, ** p<0.01, *** p<0.001. (J) ALP enzymatic activity of rMSCs induced by preosteoclast-conditioned medium from the HA and HA-BP hydrogel groups. ALP activity data are presented as the means ± SD (n=5). * p<0.05, ** p<0.01, *** p<0.001. (K) The mRNA levels of osteogenesis marker genes in rMSCs induced by preosteoclast-conditioned medium from the HA and HA-BP hydrogel groups. qPCR data are presented as the means ± SD (n=4). * p<0.05, ** p<0.01, *** p<0.001. (L) Microscopic images of cells after 5 additional days of culture on the HA and HA-BP hydrogels with a high dose of RANKL (200 ng/mL) to induce mature osteoclast differentiation. The white arrows indicate mature osteoclasts. Scale bar = 200 μm. (M) TRAP staining of mature osteoclasts cultured on the HA and HA-BP hydrogels on day 5. The red arrows indicate mature osteoclasts. Scale bar = 200 μm.

together, these results indicated that the HA-BP hydrogel could inhibit macrophages osteoclastogenesis.

3.5. The HA-BP hydrogel promotes apoptosis of RAW264.7 macrophage-derived mature osteoclasts

Bisphosphonates (BPs) have been reported to inhibit the activities of mature osteoclasts [56]. BPs can be internalized by osteoclasts and inhibit farnesyl pyrophosphate synthase (FPPS) activity, thereby reducing the synthesis of geranylgeranyl diphosphates [57,58]. This in turn inhibits protein prenylation, such as the geranylgeranylation of Rab and Rho-family GTPases, which are crucial to osteoclast activity, thereby leading to osteoclast apoptosis (Fig. 4A). Our qPCR results showed that the FPPS and geranylgeranyl diphosphate synthase (GGPPS) gene expression levels in the cells on the HA-BP hydrogel were significantly lower than those of the HA hydrogel, indicating that the HA-BP hydrogel inhibited osteoclast survival-associated gene expression (Fig. 4B). Moreover, the ELISA results suggested that the FPPS and GGPPS-catalyzed product concentrations of the HA-BP hydrogel group were significantly lower than those of the HA hydrogel group, revealing that the HA-BP hydrogel inhibited osteoclast survival-associated enzymatic activities (Fig. 4C). Finally, to assess the apoptosis of osteoclastically induced RAW264.7 macrophages cultured on the HA and HA-BP hydrogels, we used annexin V-FITC/7-AAD double-fluorescence staining. In healthy cells, phosphatidylserine is located in the inner layer of the cell membrane, and annexin V-FITC/7-AAD cannot stain these cells. In early apoptotic cells, phosphatidylserine externalizes from the inner layer to the outer layer of the cell membrane, thereby enabling binding by annexin V-FITC. In late apoptotic cells, 7-AAD can penetrate the disrupted cell membrane, and cells are simultaneously stained with annexin V-FITC and 7-AAD (Fig. 4D). After the addition of RANKL, the fluorescence intensity of annexin V-FITC in macrophages increased drastically in both the HA and HA-BP groups. Remarkably, the fluorescence intensity of 7-AAD, which stains late apoptotic cells, in the HA-BP group was significantly higher than that in the HA group, indicating a significant increase in apoptosis among mature osteoclasts in the HA-BP group (Fig. 4E). Consistent with the immunofluorescent staining, the percentage of Annexin V and 7-AAD positive cells on HA-BP hydrogel was significantly higher than that of HA hydrogel, indicating more apoptotic cells on HA-BP hydrogel (Fig. 4F and G). Taken together, these results suggested that the HA-BP hydrogel promotes the apoptosis of mature osteoclasts.

3.6. The HA- BP hydrogel supports preosteoclastic differentiation but inhibits further osteoclastic maturation of primary macrophages

Studies have shown that while mature osteoclasts mediate bone resorption, preosteoclasts are important during bone regeneration due to their secretion of PDGF-BB, coupling angiogenesis and osteogenesis [59–64]. To further evaluate the efficacy of the HA-BP hydrogel to selectively inhibit osteoclast maturation but not preosteoclast development, we derived primary macrophages by culturing monocytes harvested from the hind leg bone marrow of male C57 mice with M-CSF (Fig. 5A and Fig. S5A). Staining against F4/80, a key macrophage marker, showed that most cells were positive, indicating the monocytes have been induced to become primary macrophages successfully (Fig. S5B). The obtained primary macrophages can be further differentiated into mononuclear TRAP-positive ($TRAP^{+}$) preosteoclasts under stimulation with a low dose of RANKL [12]. There was no significant difference in the proliferation or TRAP staining intensity of preosteoclasts cultured on the HA and HA-BP hydrogels (Fig. 5B and C). In addition, the qPCR results showed that the mRNA expression levels of three markers of preosteoclasts, LY6C, CX3CR1, and Slc3a2, in the HA-BP group were not significantly different compared with those of the HA group (Fig. 5D). Furthermore, immunostaining against PDGF-B, another marker of preosteoclasts, showed that the expression level of PDGF-B in the HA-BP group was similar to that in the HA group (Fig. 5E). The quantification of PDGF-B fluorescence intensity revealed no significant difference between HA and HA-BP hydrogels (Fig. 5F). Based on the standard curve of PDGF-BB established by using ELISA (Fig. S6), there was no significant difference in PDGF-B secretion between the HA and HA-BP hydrogel group (Fig. 5G). Taken together, these data showed that the HA-BP hydrogel does not inhibit the development and PDGF-B secretion of preosteoclasts. It is noteworthy that PDGF-BB secreted by preosteoclasts induces bone regeneration [12]. Therefore, we utilized preosteoclast-conditioned medium from HA and HA-BP hydrogels to induce osteogenesis of rat mesenchymal stem cells (rMSCs). Immunostaining against ALP showed no significant difference between HA and HA-BP hydrogels (Fig. 5H and I). Based on the ALP standard curve established from the absorbance data (Fig. S7), the quantified ALP activity of the HA-BP hydrogel group was similar to that of the HA hydrogel group (Fig. 5J). In addition, the gene expressions of osteogenesis markers including Col 1 and ALP by of rMSCs of the HA-BP hydrogel group were not significantly different from those of the HA hydrogel group (Fig. 5K). Collectively, these findings demonstrated that HA-BP hydrogel did not inhibit the development of preosteoclasts from the seeded primary macrophages and the associated secretion of pro-osteogenic factors such as PDGF-B.

Upon switching to a high dose of RANKL, preosteoclasts can be further differentiated into mature osteoclasts under normal conditions (Fig. 5A). The microscopic images showed normal differentiation of mature osteoclasts with sustained TRAP activity staining in the HA hydrogel group after 5 additional days of culture with a high dose of RANKL in the medium (Fig. 5L and G). However, the density of cells on the HA-BP hydrogel decreased significantly after supplementation with a high dose of RANKL in the medium (Fig. 5L). Consistent with this

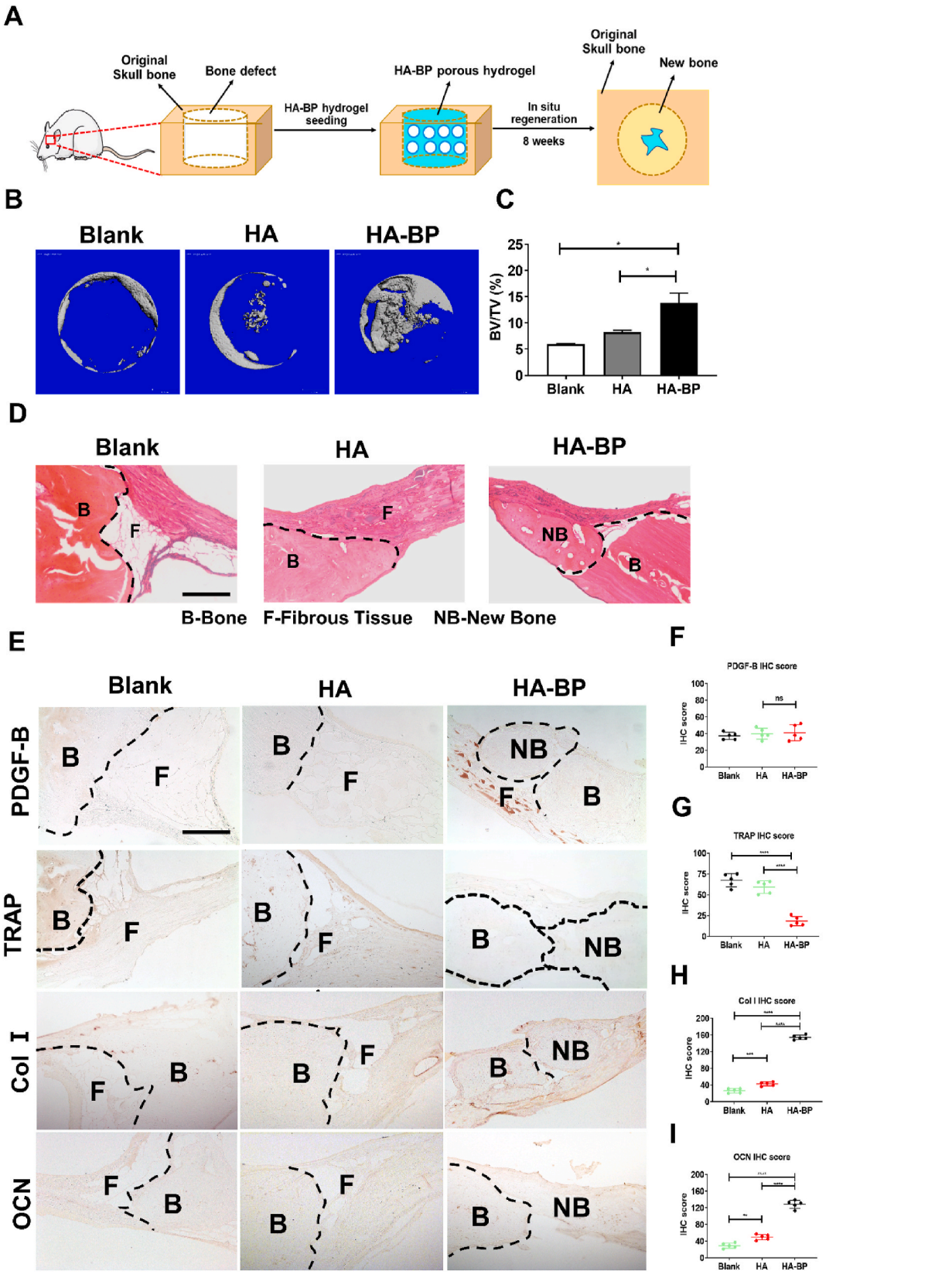

(caption on next page)

Fig. 6. The HA-BP hydrogel promotes bone regeneration in vivo. (A) Implantation of HA-BP hydrogels in critical-sized skull bone defects in rats. The BP-free HA hydrogel and nontreatment group (blank) were used as control groups. (B) Micro-CT images of bone defects in the blank, HA, and HA-BP groups obtained 8 weeks after implantation. (C) Bone volume fraction in the blank, HA, and HA-BP groups determined 8 weeks after implantation. BV, bone volume. TV, total volume. Bone volume fraction data are presented as the mean ± SD (n = 3). *p < 0.05, **p < 0.01, ***p < 0.001. (D) H&E staining of the bone defects in the blank, HA, and HA-BP groups 8 weeks after implantation. The black dotted lines indicate the boundaries between original native bone and fibrous tissue or new bone. B, original bone. F, fibrous tissue, NB, new bone. Scale bar = 200 μm. (E) TRAP, collagen I (Col I), and osteocalcin (OCN) immunohistochemical staining in the blank, HA, and HA-BP groups. The black dotted lines indicate the boundaries between the original bone and fibrous tissue or new bone. B, original bone. F, fibrous tissue, NB, new bone. Scale bar = 200 μm. (F) Immunohistochemical staining score of PDGF-B of the blank, HA and HA-BP hydrogel groups (n = 5). *p < 0.05, **p < 0.01, ***p < 0.001. (G) Immunohistochemical staining score of TRAP of the blank, HA and HA-BP hydrogel groups (n = 5). *p < 0.05, **p < 0.01, ***p < 0.001. (H) Immunohistochemical staining score of Col I (type I collagen) of the blank, HA and HA-BP hydrogel groups (n = 5). *p < 0.05, **p < 0.01, ***p < 0.001. (I) Immunohistochemical staining score of OCN (osteocalcin) of the blank, HA and HA-BP hydrogel groups (n = 5). *p < 0.05, **p < 0.01, ***p < 0.001.

finding, TRAP staining indicated a substantial decline in the TRAP activity of the cells on the HA-BP hydrogels (Fig. 5M). It should be noted that the HA-BP hydrogel also releases magnesium ions, which have been reported to inhibit the differentiation of osteoclasts [65]. Therefore, the inhibitory effects of the HA-BP hydrogels on mature osteoclastic activity may be due to the concerted action of released BP and magnesium ions.

3.7. The HA-BP hydrogel promotes in situ bone regeneration in vivo

To further evaluate the efficacy of the HA-BP hydrogel to promote bone regeneration in vivo, we implanted the porous form of the hydrogels without exogenous cells in critical-sized calvarial defects in rats and evaluated bone regeneration after 8 weeks (Fig. 6A). Rheological analysis showed no significant difference in the Young's modulus between the HA and HA-BP porous hydrogels (Fig. S8). The micro-CT data showed that there was more new bone formation in the HA-BP group than in the HA hydrogel and blank (without hydrogel implantation) control groups (Fig. 6B). The bone volume fraction (BV/TV) in the HA-BP group was significantly higher than that of the other two groups, revealing that the HA-BP hydrogel group had the best bone regeneration (Fig. 6C). In addition, hematoxylin and eosin (H&E) staining showed substantially more new bone formation in the HA-BP group than in the other two groups (Fig. 6D and Fig. S9A). Immunohistochemical staining against PDGF-B indicated no significant difference in the secretion of PDGF-B between HA and HA-BP hydrogel group (Fig. 6E and F, Fig. S9B). Furthermore, TRAP immunohistochemical staining showed that there was significantly lower TRAP expression in the HA-BP group than in the other two groups, which can be attributed to the inhibitory effects of bisphosphonate on mature osteoclasts (Fig. 6E and G, Fig. S9B). Moreover, immunostaining against collagen I (Col I) and osteocalcin (OCN) revealed that there was significantly higher expression of these two bone matrix markers in the HA-BP group than in the other two groups (Fig. 6E and H–I, Fig. S9B). Collectively, these findings demonstrate that the HA-BP hydrogel effectively promotes in situ bone regeneration by inhibiting mature osteoclastic activity.

4. Conclusion

In summary, we successfully fabricated an HA-BP hydrogel that can release BP in response to acidic pH. We showed that this HA-BP hydrogel can inhibit the differentiation of RAW264.7 macrophages to mature osteoclasts via biomimetic negative feedback regulation. We further demonstrated that the HA-BP hydrogel can support preosteoclast differentiation and its associated activity but inhibits subsequent osteoclast maturation from primary macrophages, thereby resulting in enhanced in situ bone regeneration in vivo. Our findings demonstrate an effective approach to design biomimetic biomaterial scaffolds to precisely regulate osteoclastic activity for enhanced bone regeneration.

CRediT authorship contribution statement

Zhuo Li: Methodology, Validation, Visualization, Data collection, curation, Original manuscript writing and revision. **Haixing Wang:** Animal model construction, Tissue sections collection. **Kunyu Zhang:** Conceptualization, Methodology. **Boguang Yang:** Methodology, Manuscript writing suggestions. **Xian Xie:** Data curation. **Zhengmeng Yang:** Resources. **Lingchi Kong:** Resources. **Peng Shi:** Investigation. **Yuan Zhang:** Investigation. **Yi-Ping Ho:** Investigation. **Zhi-Yong Zhang:** Conceptualization, Investigation. **Gang Li:** Conceptualization, Investigation. **Liming Bian:** Conceptualization, Funding acquisition, Investigation, Project administration, Supervision, Writing – review & editing.

Declaration of competing interest

The authors confirm that there are no conflicts of interest associated with this publication.

Acknowledgements

This project is supported by theGeneral Research Fund grants from the Research Grants Council of Hong Kong (14120118, 14202920 and 14204618). The work was partially supported by Hong Kong Research Grants Council Theme-based Research Scheme (Ref. T13-402/17-N and AoE/402/20).

Appendix A. Supplementary data

Supplementary data to this article can be found online at https://doi.org/10.1016/j.bioactmat.2021.11.004.

Data availability

The data that support the findings of this study are available from the corresponding author upon reasonable request.

References

[1] Y. Choi, J.R. Arron, M.J. Townsend, Promising bone-related therapeutic targets for rheumatoid arthritis, Nat. Rev. Rheumatol. 5 (10) (2009) 543–548.
[2] S.H. Kim, K.J. Kim, H.J. Kang, Y.J. Son, S.W. Choi, M.J. Lee, The dual role of oat bran water extract in bone homeostasis through the regulation of osteoclastogenesis and osteoblast differentiation, Molecules 23 (12) (2018).
[3] Y. Wan, PPARgamma in bone homeostasis, Trends Endocrinol. Metabol. 21 (12) (2010) 722–728.
[4] M.L. Zou, Z.H. Chen, Y.Y. Teng, S.Y. Liu, Y. Jia, K.W. Zhang, Z.L. Sun, J.J. Wu, Z. D. Yuan, Y. Feng, X. Li, R.S. Xu, F.L. Yuan, The smad dependent TGF-beta and BMP signaling pathway in bone remodeling and therapies, Front. Mol. Biosci. 8 (2021) 593310.
[5] K. Hu, B.R. Olsen, Osteoblast-derived VEGF regulates osteoblast differentiation and bone formation during bone repair, J. Clin. Invest. 126 (2) (2016) 509–526.
[6] K.S. Joeng, Y.C. Lee, J. Lim, Y. Chen, M.M. Jiang, E. Munivez, C. Ambrose, B. H. Lee, Osteocyte-specific WNT1 regulates osteoblast function during bone homeostasis, J. Clin. Invest. 127 (7) (2017) 2678–2688.
[7] N. Maruotti, A. Corrado, F.P. Cantatore, Osteoblast role in osteoarthritis pathogenesis, J. Cell. Physiol. 232 (11) (2017) 2957–2963.
[8] A. De Simone, M.N. Evanitsky, L. Hayden, B.D. Cox, J. Wang, V.A. Tornini, J. Ou, A. Chao, K.D. Poss, S. Di Talia, Control of osteoblast regeneration by a train of Erk activity waves, Nature 590 (7844) (2021) 129–133.
[9] P. Jiang, Y. Zhang, R. Hu, X. Wang, Y. Lai, G. Rui, C. Lin, Hydroxyapatite-modified micro/nanostructured titania surfaces with different crystalline phases for osteoblast regulation, Bioact. Mater. 6 (4) (2021) 1118–1129.
[10] Y. Peng, S. Wu, Y. Li, J.L. Crane, Type H blood vessels in bone modeling and remodeling, Theranostics 10 (1) (2020) 426–436.

[11] B.A. Scheven, J.S. Milne, I. Hunter, S.P. Robins, Macrophage-inflammatory protein-1alpha regulates preosteoclast differentiation in vitro, Biochem. Biophys. Res. Commun. 254 (3) (1999) 773–778.
[12] H. Xie, Z. Cui, L. Wang, Z. Xia, Y. Hu, L. Xian, C. Li, L. Xie, J. Crane, M. Wan, G. Zhen, Q. Bian, B. Yu, W. Chang, T. Qiu, M. Pickarski, L.T. Duong, J.J. Windle, X. Luo, E. Liao, X. Cao, PDGF-BB secreted by preosteoclasts induces angiogenesis during coupling with osteogenesis, Nat. Med. 20 (11) (2014) 1270–1278.
[13] P. Yang, S. Lv, Y. Wang, Y. Peng, Z. Ye, Z. Xia, G. Ding, X. Cao, J.L. Crane, Preservation of type H vessels and osteoblasts by enhanced preosteoclast platelet-derived growth factor type BB attenuates glucocorticoid-induced osteoporosis in growing mice, Bone 114 (2018) 1–13.
[14] J. Huang, Y.Y. Li, K. Xia, Y.Y. Wang, C.Y. Chen, M.L. Chen, J. Cao, Z.Z. Liu, Z. X. Wang, H. Yin, X.K. Hu, Z.G. Wang, Y. Zhou, H. Xie, Harmine targets inhibitor of DNA binding-2 and activator protein-1 to promote preosteoclast PDGF-BB production, J. Cell Mol. Med. 25 (12) (2021) 5525–5533.
[15] X. Chen, Z. Wang, N. Duan, G. Zhu, E.M. Schwarz, C. Xie, Osteoblast-osteoclast interactions, Connect. Tissue Res. 59 (2) (2018) 99–107.
[16] J. Lorenzo, The many ways of osteoclast activation, J. Clin. Invest. 127 (7) (2017) 2530–2532.
[17] T. Ono, T. Nakashima, Recent advances in osteoclast biology, Histochem. Cell Biol. 149 (4) (2018) 325–341.
[18] N.S. Soysa, N. Alles, Osteoclast function and bone-resorbing activity: an overview, Biochem. Biophys. Res. Commun. 476 (3) (2016) 115–120.
[19] B. Walia, E. Lingenheld, L. Duong, A. Sanjay, H. Drissi, A novel role for cathepsin K in periosteal osteoclast precursors during fracture repair, Ann. N. Y. Acad. Sci. 1415 (1) (2018) 57–68.
[20] C. Dou, J. Li, J. He, F. Luo, T. Yu, Q. Dai, Y. Chen, J. Xu, X. Yang, S. Dong, Bone-targeted pH-responsive cerium nanoparticles for anabolic therapy in osteoporosis, Bioact. Mater. 6 (12) (2021) 4697–4706.
[21] K. Henriksen, J. Bollerslev, V. Everts, M.A. Karsdal, Osteoclast activity and subtypes as a function of physiology and pathology-implications for future treatments of osteoporosis, Endocr. Rev. 32 (1) (2011) 31–63.
[22] K. Mostov, Z. Werb, Cell biology - journey across the osteoclast, Science 276 (5310) (1997) 219–220.
[23] C. Sobacchi, A. Schulz, F.P. Coxon, A. Villa, M.H. Helfrich, Osteopetrosis: genetics, treatment and new insights into osteoclast function, Nat. Rev. Endocrinol. 9 (9) (2013) 522–536.
[24] S.L. Teitelbaum, The osteoclast and its unique cytoskeleton, Ann. Ny Acad. Sci. 1240 (2011) 14–17.
[25] J.L. Crane, X. Cao, Function of matrix IGF-1 in coupling bone resorption and formation, J. Mol. Med. 92 (2) (2014) 107–115.
[26] N. Udagawa, M. Koide, M. Nakamura, Y. Nakamichi, T. Yamashita, S. Uehara, Y. Kobayashi, Y. Furuya, H. Yasuda, C. Fukuda, E. Tsuda, Osteoclast differentiation by RANKL and OPG signaling pathways, J. Bone Miner. Metabol. 39 (1) (2021) 19–26.
[27] K. Zhang, Z. Jia, B. Yang, Q. Feng, X. Xu, W. Yuan, X. Li, X. Chen, L. Duan, D. Wang, L. Bian, Adaptable hydrogels mediate cofactor-assisted activation of biomarker-responsive drug delivery via positive feedback for enhanced tissue regeneration, Adv. Sci. 5 (12) (2018) 1800875.
[28] K.Y. Zhang, S.E. Lin, Q. Feng, C.Q. Dong, Y.H. Yang, G. Li, L.M. Bian, Nanocomposite hydrogels stabilized by self-assembled multivalent bisphosphonate-magnesium nanoparticles mediate sustained release of magnesium ion and promote in-situ bone regeneration, Acta Biomater. 64 (2017) 389–400.
[29] K.Y. Zhang, Q. Feng, J.B. Xu, X.Y. Xu, F. Tian, K.W.K. Yeung, L.M. Bian, Self-assembled injectable nanocomposite hydrogels stabilized by bisphosphonate-magnesium (Mg2+) coordination regulates the differentiation of encapsulated stem cells via dual crosslinking, Adv. Funct. Mater. 27 (34) (2017).
[30] Y.H. Kim, X. Yang, L. Shi, S.A. Lanham, J. Hilborn, R.O.C. Oreffo, D. Ossipov, J. I. Dawson, Bisphosphonate nanoclay edge-site interactions facilitate hydrogel self-assembly and sustained growth factor localization, Nat. Commun. 11 (1) (2020) 1365.
[31] W. Yuan, Z. Li, X. Xie, Z.Y. Zhang, L. Bian, Bisphosphonate-based nanocomposite hydrogels for biomedical applications, Bioact. Mater. 5 (4) (2020) 819–831.
[32] L.Y. Shi, Y. Zhang, D. Ossipov, Enzymatic degradation of hyaluronan hydrogels with different capacity for in situ bio-mineralization, Biopolymers 109 (2) (2018).
[33] J. Bergman, A. Nordstrom, A. Hommel, M. Kivipelto, P. Nordstrom, Bisphosphonates and mortality: confounding in observational studies? Osteoporos. Int. 30 (10) (2019) 1973–1982.
[34] D. Bliuc, T. Tran, T. van Geel, J.D. Adachi, C. Berger, J. van den Bergh, J.A. Eisman, P. Geusens, D. Goltzman, D.A. Hanley, R. Josse, S. Kaiser, C.S. Kovacs, L. Langsetmo, J.C. Prior, T.V. Nguyen, J.R. Center, C.R. Grp, Reduced bone loss is associated with reduced mortality risk in subjects exposed to nitrogen bisphosphonates: a mediation analysis, J. Bone Miner. Res. 34 (11) (2019) 2001–2011.
[35] S. Cremers, M.T. Drake, F.H. Ebetino, J.P. Bilezikian, R.G.G. Russell, Pharmacology of bisphosphonates, Br. J. Clin. Pharmacol. 85 (6) (2019) 1052–1062.
[36] V.J. Mailoo, V. Srinivas, J. Turner, W.D. Fraser, Beware of bone pain with bisphosphonates, BMJ Case Rep. 12 (3) (2019).
[37] K.E. Naylor, E.V. McCloskey, R.M. Jacques, N.F.A. Peel, M.A. Paggiosi, F. Gossiel, J.S. Walsh, R. Eastell, Clinical utility of bone turnover markers in monitoring the withdrawal of treatment with oral bisphosphonates in postmenopausal osteoporosis, Osteoporos. Int. 30 (4) (2019) 917–922.
[38] C.J. Wotton, J. Green, A. Brown, M.E.G. Armstrong, S. Floud, V. Beral, G.K. Reeves, H. Abbiss, S. Abbott, R. Alison, M. Armstrong, K. Baker, A. Balkwill, I. Barnes, V. Beral, J. Black, R. Blanks, K. Bradbury, A. Brown, B. Cairns, D. Canoy, A. Chadwick, D. Ewart, S. Ewart, L. Fletcher, S. Floud, T. Gathani, L. Gerrard, A. Goodill, J. Green, L. Guiver, A. Heath, C. Hermon, D. Hogg, M. Hozak, I. Lingard, S.W. Kan, N. Langston, K. Moser, K. Pitie, A. Price, G. Reeves, K. Shaw, E. Sherman, R. Simpson, H. Strange, S. Sweetland, S. Tipper, R. Travis, L. Trickett, A. Webster, C. Wotton, L. Wright, O. Yang, H. Young, E. Banks, V. Beral, L. Carpenter, C. Dezateux, J. Green, J. Patnick, R. Peto, C. Sudlow, M.W. S. Collaborators, Use of oral bisphosphonates and risk of hospital admission with osteonecrosis of the jaw: large prospective cohort study in UK women, Bone 124 (2019) 69–74.
[39] P.R. Calvo, C.A. Sparks, J. Hochberg, K.B. Wagener, B.S. Sumerlin, Hyperbranched bisphosphonate-functional polymers via self-condensing vinyl polymerization and postpolymerization multicomponent reactions, Macromol. Rapid Commun. 42 (6) (2021), e2000578.
[40] Y. Cui, T. Zhu, D. Li, Z. Li, Y. Leng, X. Ji, H. Liu, D. Wu, J. Ding, Bisphosphonate-functionalized scaffolds for enhanced bone regeneration, Adv. Healthc. Mater 8 (23) (2019), e1901073.
[41] Y. Takagi, S. Inoue, K. Fujikawa, M. Matsuki-Fukushima, M. Mayahara, K. Matsuyama, Y. Endo, M. Nakamura, Effect of nitrogen-containing bisphosphonates on osteoclasts and osteoclastogenesis: an ultrastructural study, Microscopy (Oxf) 70 (3) (2021) 302–307.
[42] M.M. McDonald, A.S. Kim, B.S. Mulholland, M. Rauner, New insights into osteoclast biology, Jbmr Plus 5 (9) (2021).
[43] T.R. Utari, I.D. Ana, P.S. Pudyani, W. Asmara, The intrasulcular application effect of bisphosphonate hydrogel toward osteoclast activity and relapse movement, Saudi Dent. J. 33 (5) (2021) 292–298.
[44] Z.Y. Zhao, G. Li, H.T. Ruan, K.Y. Chen, Z.W. Cai, G.H. Lu, R.M. Li, L.F. Deng, M. Cai, W.G. Cui, Capturing magnesium ions via microfluidic hydrogel microspheres for promoting cancellous bone regeneration, ACS Nano 15 (8) (2021) 13041–13054.
[45] B.Y. Zhang, P.T. Yuan, G. Xu, Z.J. Chen, Z.F. Li, H.L. Ye, J.Y. Wang, P.H. Shi, X. W. Sun, DUSP6 expression is associated with osteoporosis through the regulation of osteoclast differentiation via ERK2/Smad2 signaling, Cell Death Dis. 12 (9) (2021).
[46] W. Wang, S.C. Qiao, X.B. Wu, B. Sun, J.G. Yang, X. Li, X. Zhang, S.J. Qian, Y.X. Gu, H.C. Lai, Circ_0008542 in osteoblast exosomes promotes osteoclast-induced bone resorption through m6A methylation, Cell Death Dis. 12 (7) (2021).
[47] S.X. Liu, W.P. Zhu, S.J. Li, J.C. Ma, H.T. Zhang, Z.H. Li, L. Zhang, B. Zhang, Z. Li, X. L. Liang, W. Shi, Bovine parathyroid hormone enhances osteoclast bone resorption by modulating V-ATPase through PTH1R, Int. J. Mol. Med. 37 (2) (2016) 284–292.
[48] C. Wittkowske, G.C. Reilly, D. Lacroix, C.M. Perrault, In vitro bone cell models: impact of fluid shear stress on bone formation, Front. Bioeng. Biotechnol. 4 (2016) 87.
[49] M. Roy, S. Roux, Rab GTPases in osteoclastic bone resorption and autophagy, Int. J. Mol. Sci. 21 (20) (2020).
[50] N. Takahashi, S. Ejiri, S. Yanagisawa, H. Ozawa, Regulation of osteoclast polarization, Odontology 95 (1) (2007) 1–9.
[51] K. Zhang, S. Lin, Q. Feng, C. Dong, Y. Yang, G. Li, L. Bian, Nanocomposite hydrogels stabilized by self-assembled multivalent bisphosphonate-magnesium nanoparticles mediate sustained release of magnesium ion and promote in-situ bone regeneration, Acta Biomater. 64 (2017) 389–400.
[52] J. Lin, Y. Peng, Q. Liu, K. Li, G. Lv, Y. Seimbille, G. Huang, F. Gao, L. Qiu, Pharmacological evaluation of imidazole-derived bisphosphonates on receptor activator of nuclear factor-kappaB ligand-induced osteoclast differentiation and function, Chem. Biol. Drug Des. 97 (1) (2021) 121–133.
[53] Y. Takagi, S. Inoue, K. Fujikawa, M. Matsuki-Fukushima, M. Mayahara, K. Matsuyama, Y. Endo, M. Nakamura, Effect of Nitrogen-Containing Bisphosphonates on Osteoclasts and Osteoclastogenesis: an Ultrastructural Study, Oxf), Microscopy, 2020.
[54] B. Thavornyutikarn, P.F.A. Wright, B. Feltis, W. Kosorn, T.W. Turney, Bisphosphonate activation of crystallized bioglass scaffolds for enhanced bone formation, Mater. Sci. Eng. C Mater. Biol. Appl. 104 (2019) 109937.
[55] S. Cremers, F.H. Ebetino, R. Phipps, On the pharmacological evaluation of bisphosphonates in humans, Bone 139 (2020) 115501.
[56] W. Cui, X. Chen, J. Zhu, M. Zhang, D. Xiao, X. Qin, T. Zhang, Y. Lin, Preventive effect of tetrahedral framework nucleic acids on bisphosphonate-related osteonecrosis of the jaw, Nanoscale 12 (33) (2020) 17196–17202.
[57] S. Savino, A. Toscano, R. Purgatorio, E. Profilo, A. Laghezza, P. Tortorella, M. Angelelli, S. Cellamare, R. Scala, D. Tricarico, C.M.T. Marobbio, F. Perna, P. Vitale, M. Agamennone, V. Dimiccoli, A. Tolomeo, A. Scilimati, Novel bisphosphonates with antiresorptive effect in bone mineralization and osteoclastogenesis, Eur. J. Med. Chem. 158 (2018) 184–200.
[58] B. Li, J.F. Ling Chau, X. Wang, W.F. Leong, Bisphosphonates, specific inhibitors of osteoclast function and a class of drugs for osteoporosis therapy, J. Cell. Biochem. 112 (5) (2011) 1229–1242.
[59] C. Dou, N. Ding, F. Luo, T.Y. Hou, Z. Cao, Y. Bai, C. Liu, J.Z. Xu, S.W. Dong, Graphene-based MicroRNA transfection blocks preosteoclast fusion to increase bone formation and vascularization, Adv. Sci. 5 (2) (2018).
[60] B. Gao, R.X. Deng, Y. Chai, H. Chen, B. Hu, X. Wang, S.A. Zhu, Y. Cao, S.F. Ni, M. Wan, L. Yang, Z.J. Luo, X. Cao, Macrophage-lineage TRAP(+) cells recruit periosteum-derived cells for periosteal osteogenesis and regeneration, J. Clin. Invest. 129 (6) (2019) 2578–2594.
[61] Y. Peng, S. Wu, Y.S. Li, J.L. Crane, Type H blood vessels in bone modeling and remodeling, Theranostics 10 (1) (2020) 426–436.
[62] W.P. Su, G.Q. Liu, X.N. Liu, Y.Y. Zhou, Q. Sun, G.H. Zhen, X. Wang, Y.H. Hu, P. S. Gao, S. Demehri, X. Cao, M. Wan, Angiogenesis stimulated by elevated PDGF-BB in subchondral bone contributes to osteoarthritis development, Jci Insight 5 (8) (2020).

[63] H. Xie, Z. Cui, L. Wang, Z.Y. Xia, Y. Hu, L.L. Xian, C.J. Li, L. Xie, J. Crane, M. Wan, G.H. Zhen, Q. Bian, B. Yu, W.Z. Chang, T. Qiu, M. Pickarski, L.T. Duong, J. J. Windle, X.H. Luo, E.Y. Liao, X. Cao, PDGF-BB secreted by preosteoclasts induces angiogenesis during coupling with osteogenesis, Nat. Med. 20 (11) (2014) 1270–1278.

[64] P. Yang, S. Lv, Y. Wang, Y. Peng, Z.X. Ye, Z.Y. Xia, G.X. Ding, X. Cao, J.L. Crane, Preservation of type H vessels and osteoblasts by enhanced preosteoclast platelet-derived growth factor type BB attenuates glucocorticoid-induced osteoporosis in growing mice, Bone 114 (2018) 1–13.

[65] L.Z. Zheng, J.L. Wang, J.K. Xu, X.T. Zhang, B.Y. Liu, L. Huang, R. Zhang, H.Y. Zu, X. He, J. Mi, Q.Q. Pang, X.L. Wang, Y.C. Ruan, D.W. Zhao, L. Qin, Magnesium and vitamin C supplementation attenuates steroid-associated osteonecrosis in a rat model, Biomaterials 238 (2020) 119828.